Miniaturized photoacoustic probe for *in vivo* imaging of subcutaneous microvessels within human skin

Wuyu Zhang[1,2], Haigang Ma[1,2], Zhongwen Cheng[1,2], Zhiyang Wang[1,2], Lan Zhang[3], Sihua Yang[1,2]

[1]MOE Key Laboratory of Laser Life Science & Institute of Laser Life Science, College of Biophotonics, South China Normal University, Guangzhou 510631, China; [2]College of Biophotonics, South China Normal University, Guangzhou 510631, China; [3]GMU-GIBH Joint School of Life Sciences, Guangzhou Medical University, Guangzhou 511436, China

Correspondence to: Sihua Yang. MOE Key Laboratory of Laser Life Science & Institute of Laser Life Science, South China Normal University, 55 Zungsaan Avenue West, Guangzhou 510631, China. Email: yangsh@scnu.edu.cn.

Background: Subcutaneous microvascular visualization is important for accurate diagnosis and precise treatment of those diseases that are associated with subcutaneous microangiopathy. Pure optical imaging technology and ultrasound imaging technology are commonly used to observe subcutaneous blood vessels non-invasively. However, pure optical imaging is limited to visualizing superficial skin features due to the strong scattering of light by biological tissues, while ultrasound imaging which can detect deep tissues has poor resolution and low contrast to reveal microvascular networks. This results in a lack of intuitive understanding of the disease lesion.

Methods: A miniaturized photoacoustic (PA) probe, which is capable of imaging subcutaneous microvessels with high resolution and deep penetration, was built in this work. The probe is small enough to be hand-held and takes 16 seconds to obtain a maximum amplitude projection image of 400×400 pixels with the imaging area of 2×2 mm^2.

Results: The miniaturized PA probe was measured to have a lateral resolution of about 8.9 μm and an imaging depth of about 2.4 mm. Besides, *in vivo* animal experiments and human skin imaging have been implemented. The results show that the miniaturized PA probe not only visualizes the subcutaneous microvessels, but also obtains quantitative information such as the diameters and the depths of blood vessels.

Conclusions: The miniaturized PA probe has potential been used into clinic, and providing quantitative blood vessel information for the diagnosis and monitoring of vascular diseases.

Keywords: Photoacoustic microscopy (PAM); miniaturized photoacoustic probe (miniaturized PA probe); *in vivo* skin imaging

Introduction

Many diseases, such as port wine stains and oral cancer, are accompanied by symptoms of subcutaneous microvascular diseases (1-4). The development of treatment protocols and the evaluation of treatment effects can be aided by observing the vascular morphology of the diseased area. Therefore, an effective and non-invasive medical imaging technology is necessary.

In the field of traditional medical imaging, ultrasound imaging technology and pure optical imaging technology are commonly used to observe subcutaneous blood vessels non-invasively. Ultrasound imaging technology uses the difference in acoustic impedance of biological tissue to distinguish different biological tissue structure (5). However, ultrasound images are low-contrast and non-specific. Besides, since the lateral resolution of ultrasound image depends largely on the size of the ultrasonic

transducer elements, if high spatial resolution is required, ultrasound transducer elements need to be made small, which is demanding for manufacturing process and difficult to implement. Therefore, the ultrasound imaging technology currently used clinically is usually difficult to obtain high-resolution images of subcutaneous microvessels. Pure optical imaging technology uses light scattering to reveal subcutaneous microvessels, and by focusing the detecting light, high-resolution images can be obtained (6,7). However, due to the high scattering of light by biological tissues, pure optical imaging technology usually has a shallow imaging depth, which limits the application range. The above problems result in the fact that the diagnosis of the disease often rely on the doctor's experience. It is not conducive to achieve accurate diagnosis and precision treatment. Therefore, a non-invasive imaging technique, which has high specificity of blood vessels and deep penetration, is needed.

Photoacoustic imaging (PAI) technology combines the features of pure optical imaging and ultrasound imaging. After short pulse lights (the pulse width is of nanosecond level) of a specific wavelength are absorbed by the sample, photoinduced ultrasound, named photoacoustic (PA) signals, will be generated (8,9). The ultrasonic transducer converts the PA signals into electrical signals, which are acquired by the data acquisition (DAQ) system and ultimately reconstructed into images by a computer. Unlike pure optical imaging and ultrasound imaging, PAI is based on the specific optical absorption of target, which makes it more easily obtain high-specificity and high-contrast images in a non-invasive manner. This is a big advantage of PAI in the field of medical imaging. Besides, PA signals have better tissue permeability than light, so the imaging depth of PAI can be deeper than that of the pure optical imaging. Due to the above advantages, PAI is widely used in biomedical research, such as early tumor detection and blood oxygen saturation measurement (8-12).

As an important branch of PAI, photoacoustic microscopy (PAM) is commonly used to obtain high-resolution images of blood vessels within biological tissues. PAM systems obtain images by raster scanning. Some of them scan the focused light or the focused ultrasound transducer, while others scan the sample (13,14). The axial resolution of PAM, which is determined by the ultrasonic detector, can be estimated with the formula: $0.88\,c/B$, where c is the sound speed of water (1,500 m/s), and B is the bandwidth of the ultrasonic transducer (15). The lateral resolution of PAM is determined by the bigger one between the focal spot size and the scanning step. According to the determinants of lateral resolution, PAM is divided into two modes: acoustic-resolution PAM (AR-PAM) and optical-resolution PAM (OR-PAM). The lateral resolution of AR-PAM can reach tens of microns and the imaging depth can reach more than 5 mm (13,14). The lateral resolution of OR-PAM can reach micron levels, and the imaging depth is usually within 3 mm (15-21).

In recent years, many novel OR-PAM systems have been reported. Hajireza *et al.* (22) built a real-time handheld OR-PAM system by fast scanning mirrors and an image guide with 30,000 fiber pixels. Chen *et al.* (23), Lin *et al.* (24) and Park *et al.* (25) used two-axis magnetic MEMS scanners to build handheld OR-PAM systems with fast imaging speed. Combined with the advantages of the small size and fast imaging speed of above systems, in this paper, a miniaturized photoacoustic probe with the position of the light focus adjustable, which can be hand-held and can image narrow portions (such as lips), was built. It was used to image the subcutaneous microvessels at human lips and skin, and obtained quantitative information such as the diameters and the depths of blood vessels. Compared with the PAM system used in our past works (26-31), the miniaturized photoacoustic probe has the characteristics of small volume and fast imaging speed, which makes it more suitable for the detection of subcutaneous microvessels in various parts of the human body. The miniaturized photoacoustic probe has clinical potential for the diagnosis and monitoring of vascular diseases.

Methods

Imaging system

Figure 1 shows the schematic of the PAM system. Laser light is emitted at a maximum repetition rate of 10 kHz by a 532 nm pulsed laser (DTL-314QT, Laser-export). The laser is filtered and then coupled by a fiber coupler (PAF2-7A, Thorlabs) to a single mode fiber (SMF) with a core diameter of 4 microns, and transmitted by the fiber to a fiber collimator (F240FC-532, Thorlabs). The collimated light is reflected and scanned by an FPGA-driven fast two-dimensional galvanometer scanner (S-8107, Sunny Technology) and then focused by a plan achromat objective (RMS4, Thorlabs). Adjusting the adjustment stage allows the optical focus to be set in the surface of the target and the center of the ultrasound transducer receiving area. A transparent glass sheet, which is tilted at an angle of 45°,
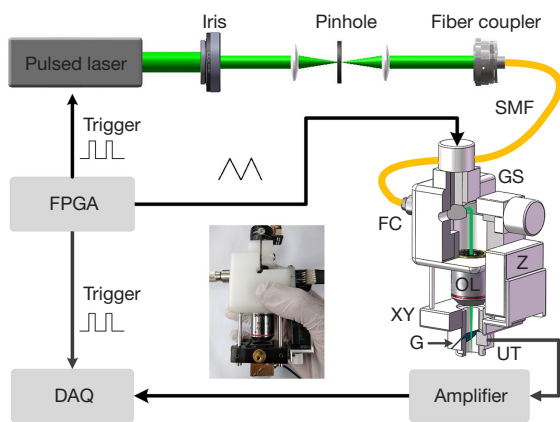
Figure 1 The schematic of the photoacoustic microscopy system. SMF, single mode fiber; GS, galvanometer scanner; FC, fiber collimator; OL, objective lens; Z, Z-direction stage; XY, XY-direction stage; G, glass; UT, ultrasound transducer; DAQ, data acquisition; FPGA, field-programmable gate array.

reflects the PA signals to a planar ultrasonic transducer with effective aperture of 5 mm and center frequency of 15 MHz. Water, as the ultrasonic coupling medium, is sealed in the probe by transparent films.

DAQ and processing

The detected PA signals are amplified with a 50 dB low noise amplifier (LNA-650, RFBAY) and then digitized with a DAQ card (sampling rate 200 M samples/second, SPECTRUM).

The reconstruction of the point-to-point maximum amplitude projection (MAP) image is realized by LABVIEW (National Instruments) and MATLAB (Math Works) programs. After the PA data collected by the DAQ card is bandpass filtered to remove high frequency and low frequency noise, the processed data is imaged. In a PA MAP image, each pixel corresponds to the maximum value of the PA signal excited by one laser pulse. Limited by the repetition rate (10 kHz) of laser, it takes 16 seconds for the miniaturized photoacoustic probe to obtain a MAP image of 400×400 pixels. The imaging area is 2×2 mm^2 (each pixel corresponds to 5×5 μm^2) and the imaging speed of B-scan is 25 frames per second.

The ESF curves are obtained by the Boltzmann fitting function of the Origin. Then, the LSF curve is obtained by calculating the first derivative of the ESF curve.

The depth-coded image in this work is realized by the following process: the three-dimensional (3D) data obtained is sliced layer by layer in the depth direction by the LABVIEW program; the obtained images are imported into the ImageJ (National Institutes of Health) software; the depth-coded image is obtained by the function provided by the software. The 3D view and edge-extracted images are obtained by the ImageJ, too.

To measure the diameters of the blood vessels, firstly, a vessel of interest is selected from the obtained PA MAP image. Then the distance between two boundaries of it at the cross section, which is vertical to the direction of the vessel, is measured by the ImageJ.

Using the method mentioned above, the diameters of all the blood vessels at different depths are measured separately. Then the average values of the blood vessel diameters of different depths are obtained.

In vivo animal experiment

In order to prove the ability of the miniaturized photoacoustic probe to reveal the microvascular networks, *in vivo* imaging of a Leghorn rooster's wattle was performed. During the experiment, the Leghorn rooster was not anesthetized because the imaging speed was fast enough to obtain a complete image. During the *in vivo* experiments, the energy at the focus of a single laser pulse was about 80 nJ. Due to the scattering of light by the epidermis, the light intensity of the 532 nm laser on the tissue surface was within the American National Standards Institute's safety limits (20 mJ/cm^2). No obvious damage was observed after the experiments.

In vivo human experiment

In order to demonstrate the clinical potential of the miniaturized photoacoustic probe, the lower lip and the wrist of human were imaged *in vivo*. During the experiment, Asian male volunteers sat in chairs and wore goggles to avoid potential laser damage. After the experiment, the clinician examined the imaging area and no obvious damage was found. The consents of volunteers were obtained and all procedures were approved by South China Normal University.

Results

To obtain the best performance index of the miniaturized photoacoustic probe, the experiments shown in *Figure 2*
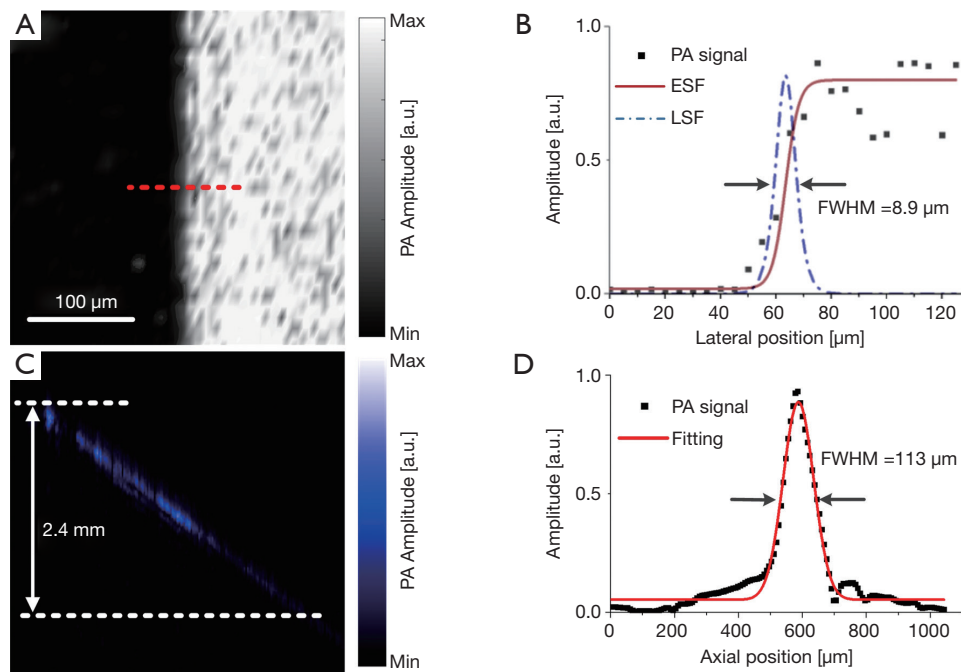
Figure 2 Evaluation of the system performance. (A) The PA MAP image of the sharp blade; (B) estimation of the lateral resolution of the system; (C) B-Scan image of a diagonally inserted carbon rod in phantom; (D) estimation of the axial resolution of the system.
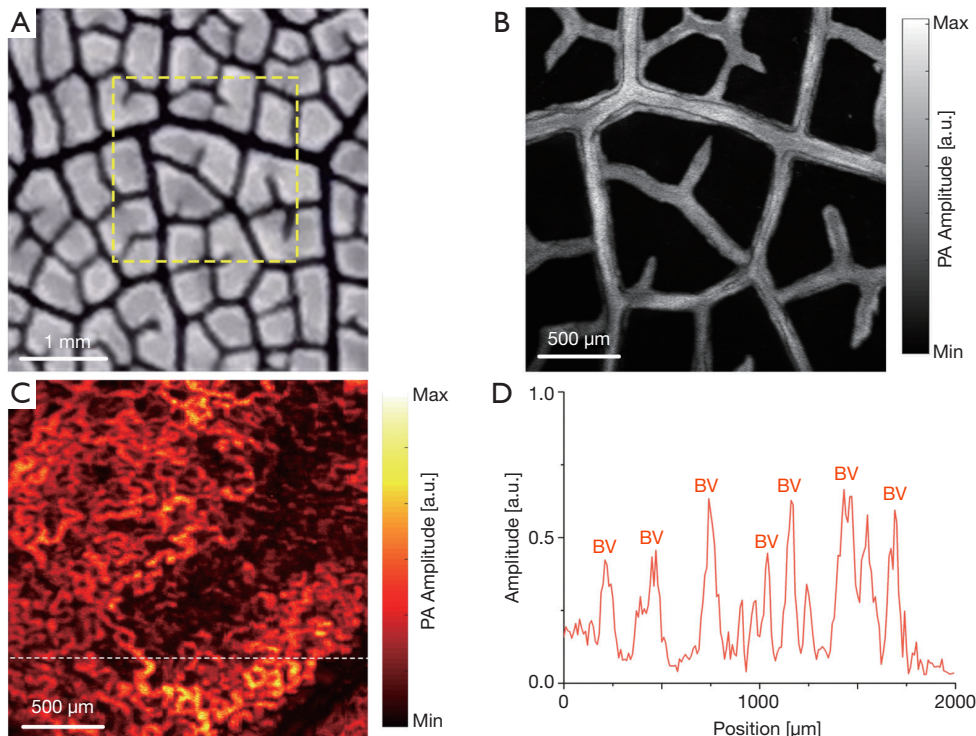
Figure 3 Experiments of phantoms and animals to prove the imaging ability of the microvascular networks. (A) The photo of a leaf vein which was dyed black. (B) The PA MAP image of a 2×2 mm^2 area, which is in the yellow dashed box of (A). (C) The PA MAP image of a Leghorn rooster's wattle *in vivo*. (D) The curves of PA signal amplitude corresponding to the dashed line in (C). BV, blood vessels.
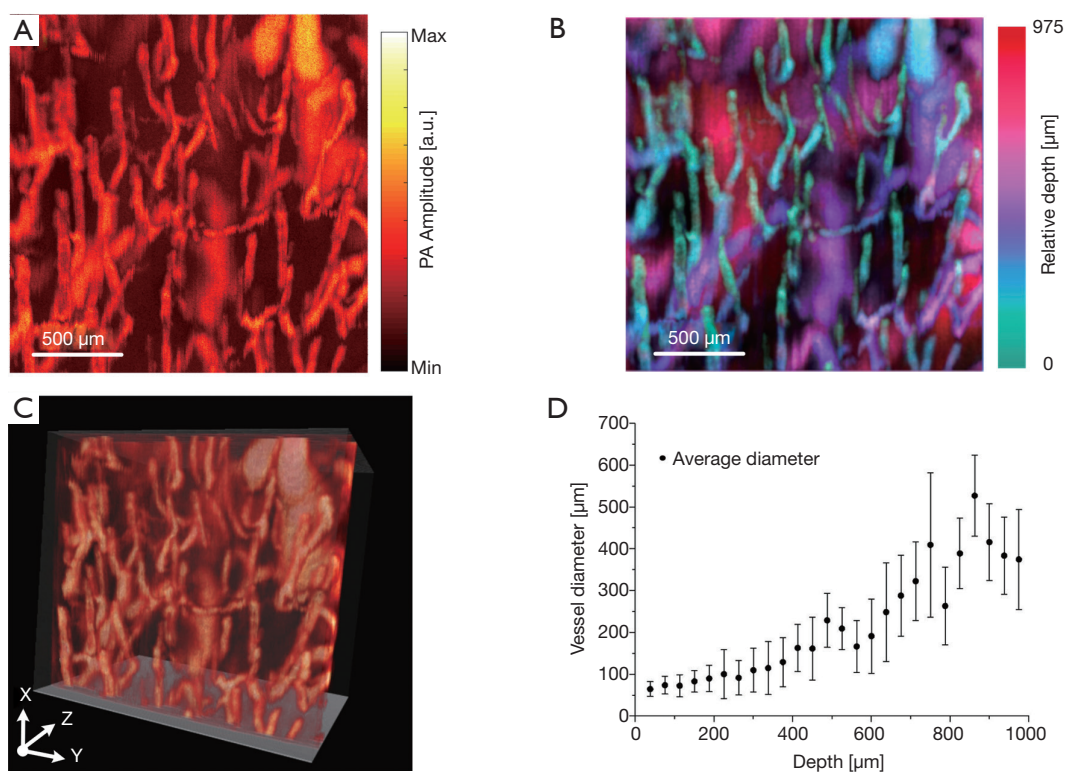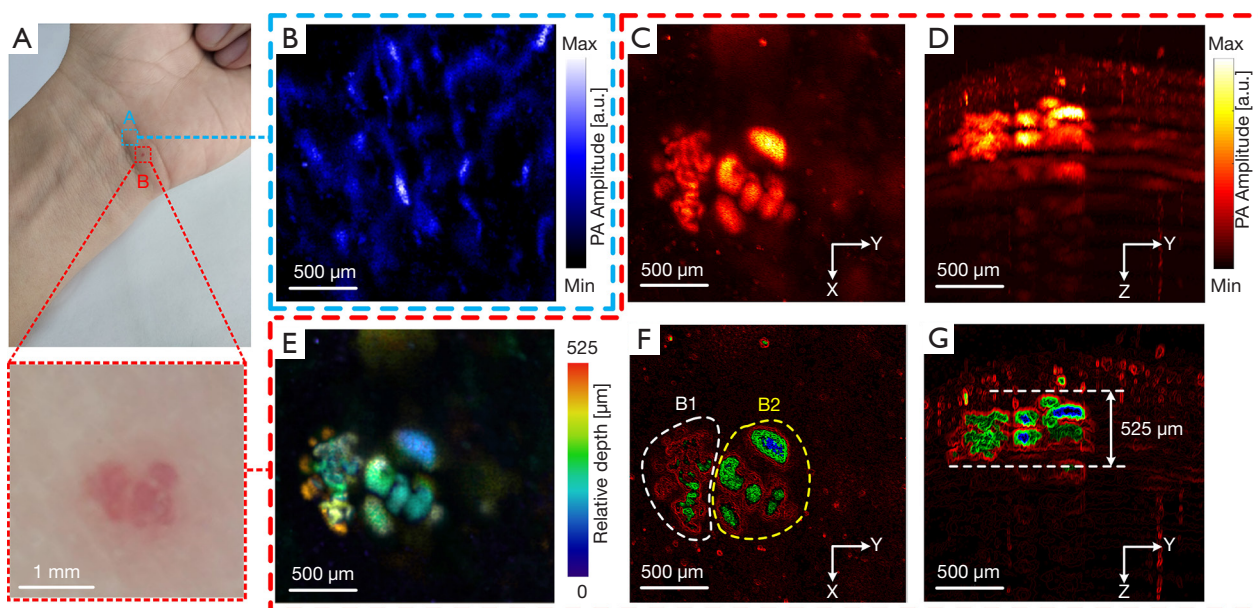
Figure 4 *In vivo* imaging of subcutaneous blood vessels of an Asian human lower lip. (A) The PA MAP image of subcutaneous vasculatures at an Asian human lower lip; (B) the depth-coded image of (A); (C) the 3D view of (A); (D) the average diameters of blood vessels at different depths.

were performed. *Figure 2A* shows the MAP image of a sharp blade. To estimate the lateral resolution, the contour along the red dashed line was fitted to obtain the edge spread function (ESF) curve, which was used to derive the line spread function (LSF) curve, as shown in *Figure 2B*. The lateral resolution was measured to be ~8.9 µm by calculating the full width at half maximum (FWHM) of the LSF curve. *Figure 2C* shows the B-scan image of the obliquely inserted carbon rod in agar phantom. It can be seen that the imaging depth can be up to ~2.4 mm. *Figure 2D* shows the Gaussian fitting axial profile of a typical PA A-line signal (after the Hilbert transform). The FWHM is about 113 µm, which indicates the axial resolution of the system.

In order to prove the ability of the miniaturized photoacoustic probe to reveal the microvascular networks, the experiments shown in *Figure 3* were performed. The imaging accuracy of the miniaturized photoacoustic probe was demonstrated in *Figures 3A,B*. *Figure 3A* is a partial enlarged photograph of a leaf vein which was dyed black. *Figure 3B* shows a PA MAP image of the yellow dashed box area of *Figure 3A*, where the details of the leaf vein can be seen. It can be seen that the imaging results accurately exhibit the morphology

and structure of the sample. Then, a Leghorn rooster's wattle was imaged *in vivo*. *Figure 3C* presents a PA MAP image of the vascular network of the wattle. *Figure 3D* is the PA amplitude curve at the dashed line in *Figure 3C*.

In order to verify the ability of miniaturized photoacoustic probe to reveal subcutaneous microvessels within human skin, and to further verify the clinical potential to help in the diagnosis and monitoring of vascular diseases, the experiments shown in *Figures 4* and *5* were performed. *Figure 4A* presents a PA MAP image of the vascular network at the lower lip of an Asian human. From this, blood vessels of different diameters can be identified. *Figures 4B,C*, which visually show the relative depth relationship of the vascular network, are respectively the depth-coded image and the 3D view of the vascular network at the lower lip in *Figure 4A*. In addition, by measuring and counting layer by layer, the average diameters of the blood vessels and the depths of the blood vessels can be obtained, as shown in *Figure 4D*. This proves that the miniaturized photoacoustic probe can show the spatial distribution of blood vessels while imaging the microvessels within human skin. During the experiment, since the detection window was inclined at an angle to

Figure 5 *In vivo* imaging of subcutaneous blood vessels at an Asian human wrist. (A) The photograph of the imaging area, where A is the normal skin and B is a vascular nevus; (B) the PA MAP image of the imaging area A; (C) the PA MAP image of the imaging area B; (D) the side view MAP image of the imaging area B; (E) the depth-coded image of (C); (F) the edge-extracted image of (C); (G) the edge-extracted image of (D).

the growth direction of the blood vessels, some vessels aligned vertically in the results. And some blood vessels exceeded the detection depth, which caused them to appear discontinuous. In order to ensure that the detection window was in close contact with the surface of the lip, we applied a certain pressure to the lip in the experiment. However, the pressure should be biased, causing some blood vessels to be closer to the transducer and in a defocused place. In addition, due to the scattering of light, the lateral resolution was deteriorated when imaging blood vessels of deep layers, which may result in that blood vessels' edges become blurry. That is why some of the blood vessels in the results were found blurred.

Figure 5A is a photograph of an Asian volunteer's wrist with normal skin in the blue dashed box (A) and blood vessels in the dashed red box (B). *Figures 5B,C* are PA MAP images of the normal region (A) and the vascular nevus (B), respectively. *Figures 5D,E* are the side view PA MAP image and the depth-coded image of the vascular nevus, respectively. It should be specially noted that due to the dense blood vessels in the vascular nevus, which lead to the high hemoglobin concentration, the signal amplitude of the diseased area is much higher than that of the surrounding normal blood vessels. Then the pixel values

of the surrounding normal blood vessel signals are pulled down, displayed as black background. *Figures 5F,G* are edge-extracted images of the diseased area in *Figures 5C,D*, respectively. The different colors in *Figures 5F,G* are used to distinguish edges. From *Figure 5F*, it can be seen that the vascular structure of the region B1 and the vascular structure of the region B2 are completely different. The blood vessels of the region B1 are small and dense, but the blood vessels of the region B2 are large and sparse. This proves that the miniaturized photoacoustic probe can distinguish different morphological features of microvessels.

As seen from *Figure 5*, the morphologies of subcutaneous blood vessels in the normal and the diseased skin area are significantly different, and the size and thickness of the diseased area can be obtained. It proves that the miniaturized photoacoustic probe can visualize the subcutaneous microvessels with high resolution and high contrast, which is helpful in the diagnosis and monitoring of vascular diseases.

Discussion and conclusions

In this work, a miniaturized photoacoustic probe for *in vivo* imaging of subcutaneous microvessels within human skin

was developed. The performance of the system was assessed using experiments of phantoms, animal and human skin imaging. Results show that the miniaturized photoacoustic probe can obtain quantitative information while visualizing blood vessels, which is a great help for the diagnosis and monitoring of vascular diseases. However, there are still some limitations. First, the imaging area is small, which is mainly caused by the size of the transducer. To expand the imaging area, a transducer with a large effective aperture can be selected. Second, the axial resolution needs to be improved. In theory, the axial resolution depends on the center frequency and bandwidth of the ultrasonic transducer. Therefore, better axial resolution can be achieved by using a high frequency transducer with a wide bandwidth. Third, the imaging speed of the system is limited by the repetition rate of the laser. If a laser with high repetition rate is applied, real-time imaging can be achieved, which will greatly facilitate the promotion of PAM in clinical applications. All in all, the miniaturized photoacoustic probe will be better used in clinical applications after overcoming various difficulties.

Acknowledgments

Footnote

Conflicts of Interest: The authors have no conflicts of interest to declare.

Ethical Statement: The consents of volunteers were obtained and all procedures were approved by South China Normal University.

References

1. Barsky SH, Rosen S, Geer DE, Noe JM. The nature and evolution of port wine stains: A computer-assisted study. J Invest Dermatol 1980;74:154-7.

2. Regezi JA, Sciubba J, Jordan RCK. Oral pathology: clinical pathologic correlations. St. Louis: Elsevier, 2008.

3. Scully C, Bagan JV, Hopper C, Epstein JB. Oral cancer: current and future diagnostic techniques. Am J Dent 2008;21:199-209.

4. Neville BW, Day TA. Oral cancer and precancerous lesions. CA Cancer J Clin 2002;52:195-215.

5. Smith SW, Pavy HG, Von Ramm OT. High-speed ultrasound volumetric imaging system. I. Transducer design and beam steering. IEEE Trans Ultrason Ferroelectr Freq Control 1991;38:100-8.

6. Wang RK, Jacques SL, Ma Z, Hurst S, Hanson SR, Gruber A. Three dimensional optical angiography. Optics Express 2007;15:4083-97.

7. An L, Shen TT, Wang RK. Using ultrahigh sensitive optical microangiography to achieve comprehensive depth resolved microvasculature mapping for human retina. J Biomed Opt 2011;16:106013.

8. Wang LV, Hu S. Photoacoustic tomography: in vivo imaging from organelles to organs. Science 2012;335:1458-62.

9. Wang Y, Xing D, Zeng Y, Chen Q. Photoacoustic imaging with deconvolution algorithm. Phys Med Biol 2004;49:3117-24.

10. Yuan Z, Jiang H. Quantitative photoacoustic tomography: Recovery of optical absorption coefficient maps of heterogeneous media. Applied Physics Letters 2006;88:231101.

11. Jathoul AP, Laufer J, Ogunlade O, Treeby B, Cox B, Zhang E, Johnson P, Pizzey AR, Philip B, Marafioti T, Lythgoe MF, Pedley RB, Pule PA, Beard P. Deep in vivo photoacoustic imaging of mammalian tissues using a tyrosinase-based genetic reporter. Nature Photonics 2015;9:239-46.

12. Li L, Zhu L, Ma C, Lin L, Yao J, Wang L, Maslov K, Zhang R, Chen W, Shi J, Wang LV. Single-impulse panoramic photoacoustic computed tomography of small-animal whole-body dynamics at high spatiotemporal resolution. Nat Biomed Eng 2017;1:0071.

13. Aguirre J, Schwarz M, Garzorz N, Omar M, Buehler A, Eyerich K, Ntziachristos V. Precision assessment of label-free psoriasis biomarkers with ultra-broadband optoacoustic mesoscopy. Nat Biomed Eng 2017;1:0068.

14. Wang LV, Yao J. A practical guide to photoacoustic tomography in the life sciences. Nat Methods 2016;13:627-38.

15. Wang Y, Xu D, Yang S, Xing D. Toward in vivo biopsy of melanoma based on photoacoustic and ultrasound dual

imaging with an integrated detector. Biomed Opt Express 2016;7:279.

16. Wong TTW, Zhang R, Zhang C, Hsu HC, Maslov KI, Wang L, Shi J, Chen R, Shung KK, Zhou Q, Wang LV. Label-free automated three-dimensional imaging of whole organs by microtomy-assisted photoacoustic microscopy. Nat Commun 2017;8:1386.

17. Jin T, Guo H, Jiang H, Ke B, Xi L. Portable optical resolution photoacoustic microscopy (pORPAM) for human oral imaging. Optics Letters 2017;42:4434-7.

18. Lan B, Liu W, Wang Y, Shi J, Li Y, Xu S, Sheng H, Zhou Q, Zou J, Hoffmann U, Yang W, Yao J. High-speed widefield photoacoustic microscopy of small-animal hemodynamics. Biomed Opt Express 2018;9:4689-701.

19. Jiang B, Yang X, Luo Q. Reflection-mode Bessel-beam photoacoustic microscopy for in vivo imaging of cerebral capillaries. Optics Express 2016;24:20167-76.

20. Guo Z, Li G, Chen S. Miniature probe for all-optical double gradient-index lenses photoacoustic microscopy. J Biophotonics 2018;e201800147.

21. Zhao L, Yang M, Jiang Y, Li C. Optical fluence compensation for handheld photoacoustic probe: An in vivo human study case. Journal of Innovative Optical Health Sciences 2017;10:1740002.

22. Hajireza P, Shi W, Zemp RJ. Real-time handheld optical-resolution photoacoustic microscopy. Optics Express 2011;19:20097-102.

23. Chen Q, Guo H, Jin T, Qi W, Xie H, Xi L. Ultracompact high-resolution photoacoustic microscopy. Optics Letters 2018;43:1615-8.

24. Lin L, Zhang P, Xu S, Shi J, Li L, Yao J, Wang L, Zou J, Wang LV. Handheld optical-resolution photoacoustic microscopy. Journal of Biomedical Optics 2017;22:41002.

25. Park K, Kim JY, Lee C, Jeon S, Lim G, Kim C. Handheld Photoacoustic Microscopy Probe. Scientific Reports 2017;7:13359.

26. Yuan Y, Yang S, Xing D. Optical-resolution photoacoustic microscopy based on two-dimensional scanning galvanometer. Applied Physics Letters 2012;100:023702.

27. Chen Z, Yang S, Xing D. In vivo detection of hemoglobin oxygen saturation and carboxyhemoglobin saturation with multiwavelength photoacoustic microscopy. Optics Letters 2012;37:3414-6.

28. He G, Li B, Yang S. In vivo imaging of a single erythrocyte with high-resolution photoacoustic microscopy. Frontiers of Optoelectronics 2015;8:122-7.

29. Xu D, Yang S, Wang Y, Gu Y, Xing D. Noninvasive and high-resolving photoacoustic dermoscopy of human skin. Biomed Opt Express 2016;7:2095.

30. Ma H, Yang S, Cheng Z, Xing D. Photoacoustic confocal dermoscope with a waterless coupling and impedance matching opto-sono probe. Optics Letters 2017;42:2342-5.

31. Ma H, Cheng Z, Wang Z, Gu Y, Zhang T, Qiu H, Yang S. Fast linear confocal scanning photoacoustic dermoscopy for non-invasive assessment of chromatodermatosis. Applied Physics Letters 2018;113:083704.